MATERIALS CHEMISTRY
FRONTIERS

RESEARCH ARTICLE

View Article Online
View Journal

Cite this: DOI: 10.1039/d5qm00845j

Tuning macrocyclic thermoelectrics *via* thiophene regioisomerism

Mona Alshammari,†[ab] Asma Alajmi,†[ca] Bashayr Alanazi,[da] Alotaibi Hanadi,[ae] Adel Alrehaili,[af] Alaa Al-Jobory,[a] Colin Lambert[a] and Ali Ismael*[ag]

Quantum interference (QI) in single-molecule junctions exhibits robust effects at room temperature, which can be intuitively modeled using quantum circuit rules (QCR) and magic ratio (MR) theory. These frameworks describe how molecular conductance is governed by constituent moieties and their connectivity. Here, we apply these principles to explore the thermoelectric properties of a series of macrocyclic structures featuring multiple electron pathways, with mixed *meta* and *para* connectivities. Our density functional theory (DFT) calculations rationalize the experimentally measured conductance trends, demonstrating excellent agreement between theory and experiment. Furthermore, we predict that these macrocyclic junctions achieve significantly higher Seebeck coefficients than conventional single-branched analogues. A key finding is that strategic repositioning of sulfur atoms within the thiophene rings enables fine tuning of QI, modulating conductance and thermoelectric performance. Our work establishes macrocyclic architectures with tunable connectivities as a highly promising platform for advanced molecular thermoelectrics.

Received 26th November 2025,
Accepted 22nd February 2026

DOI: 10.1039/d5qm00845j

rsc.li/frontiers-materials

1. Introduction

Electron transport through a single molecule connected to source and drain electrodes is strongly influenced by quantum interference (QI), even at room temperature.[1–13] Over recent years, attention has increasingly turned toward leveraging QI to fine-tune electrical current within individual molecular components. For example (see Fig. 1), the quantum mechanical wave behavior of electrons explains the reduced electrical conductance observed in *meta*-connected benzene molecules, compared with the higher-conductance of *para*-connected molecules.[14–18] Fundamentally, QI arises when multiple transmission channels exist within a molecule either through spatially distinct paths or *via* frontier molecular orbitals. Depending on the phase alignment of these paths, constructive quantum interference (CQI) or destructive quantum interference (DQI) can occur, leading to high or low conductance respectively.[19–28] This understanding has led to innovative designs of devices at the molecular scale, including wires,[29,30] switches,[31–34] and thermoelectric systems.[35–37] Factors like substitution patterns, flexibility of molecular conformations, and anchoring site modifications greatly alter QI-driven transmission characteristics.[3,38,39] In light of these insights, theoretical models, such as those based on density functional theory (DFT)[40] and tight binding (*i.e.*, Hückel) approximations,[41] have become essential tools. These models have been crucial in interpreting experimental outcomes and predicting the influence of chemical modifications. By simulating changes to functional groups or anchoring locations, it is now possible to predict whether a molecule will display CQI or DQI, thereby guiding future synthesis. In the molecular electronics literature, the role of structural isomerisation in extended π-conjugated systems is commonly investigated through comparative studies of closely related molecular architectures, in

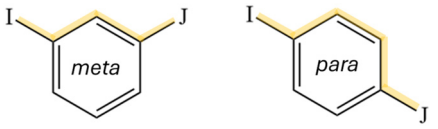

Fig. 1 Graphical representation of QI prediction applied to benzene with *meta* and SI connections to source and drain electrodes, *via* bonds labelled I and J.

[a] *Physics Department, Lancaster University, Lancaster, LA1 4YB, UK. E-mail: k.ismael@lancaster.ac.uk*
[b] *Department of Physics, College of Science, University of Hafr Al Batin, Al Jamiah District, Hafar Al Batin, 39524, Eastern Province, Saudi Arabia*
[c] *Department of Physics, College of Science and Humanities in Al-Kharj, Prince Sattam Bin Abdulaziz University, Al-Kharj, 11942, Saudi Arabia*
[d] *Department of Physics, College of Science, Northern Bord University, Arar, Saudi Arabia*
[e] *Department of Physics, College of Science and Humanities, Shaqra University, Al-Dawadimi Road, Riyadh Province, 11961, Saudi Arabia*
[f] *Physics Department, Faculty of Science, Islamic University of Madinah, Madinah, 42351, Saudi Arabia*
[g] *Department of Physics, College of Education for Pure Science, Tikrit University, Tikrit, Iraq*
† These authors contributed equally to this work.

which the overall molecular backbone, π-planarity, and number of atoms are preserved, while only a single local structural element is modified. Such an approach enables the isolation of specific structure–property relationships without introducing large-scale conformational or architectural changes.

Representative examples include metalloporphyrin molecular junctions, where replacing only the central metal atom (*e.g.*, Zn, Co, Cu or Ni) within an otherwise identical porphyrin macrocycle leads to pronounced changes in electrical conductance, despite the molecular framework remaining unchanged.[42] These studies demonstrate that meaningful insights into charge-transport mechanisms can be obtained without invoking global structural isomerisation.

Similarly, heteroatom-induced asymmetry studies have shown that modifying the position or identity of a single heteroatom within an otherwise identical π-conjugated framework can strongly influence quantum interference and charge transport, while preserving molecular length, backbone connectivity, and planarity.[43] Such controlled positional variations are widely used to probe quantum interference effects without altering the overall molecular architecture.

In line with this established methodology, the molecules investigated in the present work share the same macrocyclic backbone and π-conjugated framework, enabling a controlled comparison that isolates the effect of local connectivity rather than large-scale structural rearrangement.

In the present study, we aim to explore how QI manifests in the four macrocyclic systems shown in Fig. 2. These are labelled **BMC1**, **BMC2**, **TMC3**, and **TMC4**, where ''BMC'' denotes benzene macrocycles, while ''TMC'' refers to thiophene macrocycles. These molecules were synthesized and structurally characterized in a recent experimental study.[44] Our aim here is to present a theoretical study of these molecules and elucidate the role of QI in determining their electrical conductance and thermoelectric performance. In what follows, the thiophene rings in **TMC3** and **TMC4** will be described as *para*-connected, because it is known that these correspond to CQI connectivities.[45] After analyzing electron transport in all four molecules, we shall also consider the effect of moving the sulfur atom in these rings to alternative ring locations, which switch the QI from CQI to DQI.

2. Computational methods

Density functional theory (DFT) computations were conducted using the SIESTA package.[40,46,47] Structural optimizations of the isolated molecules were achieved by relaxing all atomic

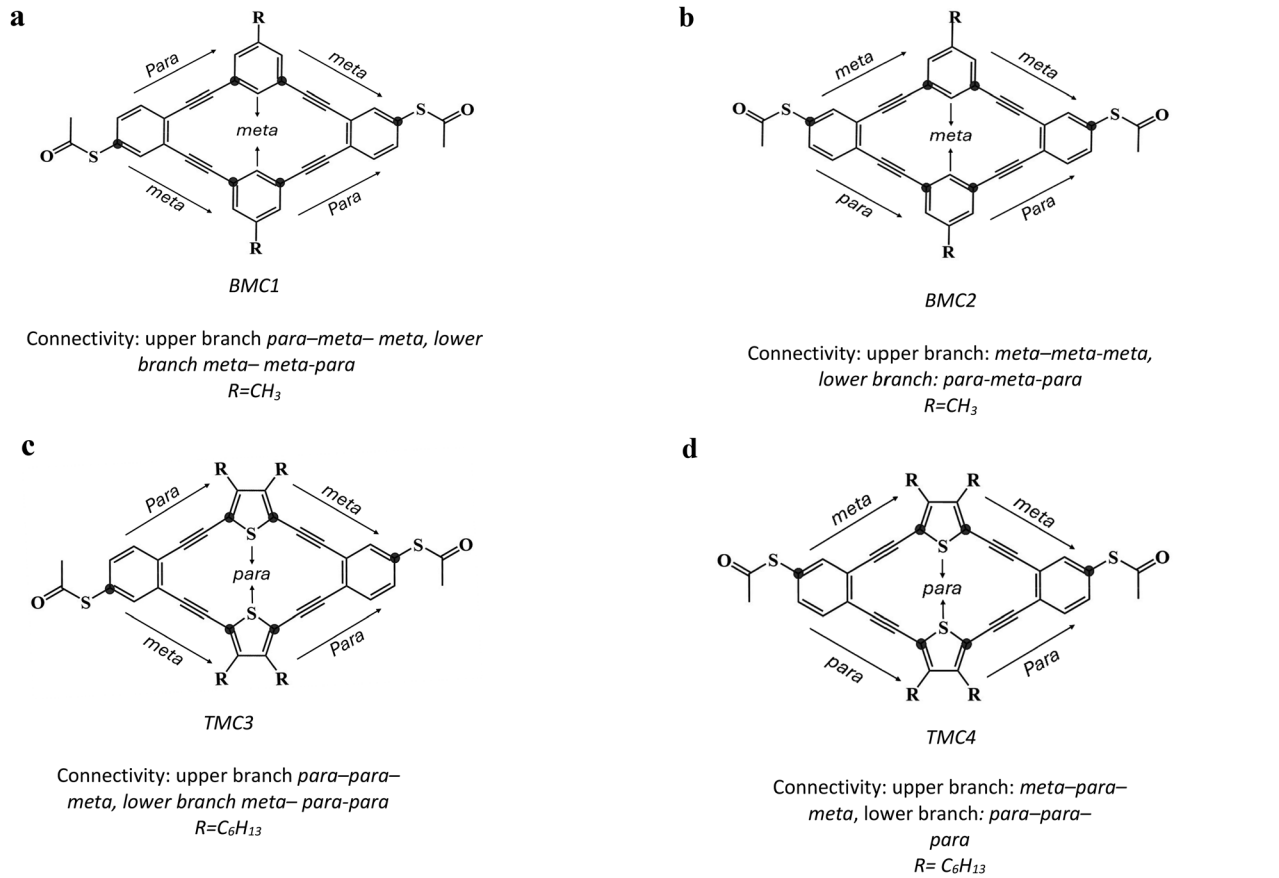

Fig. 2 Chemical structures of the studied macrocyclic molecules (MCs): (a) **BMC1** and (b) **BMC2** are benzene-based macrocycles with different branch arrangements; (c) **TMC3** and (d) **TMC4** are thiophene-based macrocycles. Terminal groups (R = CH_3 or C_8H_{13}) are shown, and the black circles indicate the anchoring positions used in electronic transport calculations. Adapted from ref. 19.

coordinates until the residual forces on each atom were reduced below 0.01 eV $Å^{-1}$. The calculations employed a double-zeta polarized basis set in combination with norm-conserving pseudopotentials and a real-space integration grid cutoff of 250 Ry. For the exchange correlation interactions, the generalized gradient approximation (GGA) was adopted.[48–50] The DFT optimized geometries were subsequently used as the input structures for quantum transport simulations. An overview of the molecular connectivity and architectures of the simulated macrocyclic compounds is presented in Fig. S1 in the SI. Table S1 provides the complete IUPAC nomenclature along with detailed structural descriptions. The fully optimised molecular geometries used in the electronic transport analysis are depicted in Fig. S2, which shows the conformations specific to each structure. Furthermore, their electronic structure was examined through frontier molecular orbital (FMO) analysis, including the highest occupied molecular orbital (HOMO), lowest unoccupied molecular orbital (LUMO), and neighboring orbitals, as illustrated in Fig. S3–S6. These FMOs reveal the spatial distribution of phase and amplitude that impacts charge transport behavior and QI effects. Each molecule is functionalised with two terminal thioacetate groups, which, after deprotection, allow two sulfur atoms to connect to electrodes and electrons to flow through the molecular framework. To investigate charge transport characteristics, we applied the non-equilibrium Green's function (NEGF) methodology *via* the Gollum quantum transport code. This method enables computation of the energy dependent transmission function $T(E)$, describing the probability that an electron of energy E can pass from one electrode to the other. From this the electrical conductance is evaluated using the Landauer formula: $G = G_0T(E_F)$,[27] where G_0 denotes the quantum of conductance. Each molecular junction was positioned between two semi-infinite gold leads, modeled as six-layer Au(111) slabs containing 30 atoms each. Terminal sulfur atoms were anchored to the gold surfaces in their most energetically favorable adsorption configurations to simulate experimentally most-probable binding geometries.

3. Results and discussion

3.1 DFT calculations

This section explores the electrical conductance characteristics of four macrocyclic molecules **BMC1**, **BMC2**, **TMC3**, and **TMC4** using DFT. We begin by analysing how different *para*- and *meta*-connectivity patterns affect QI within the cyclic structures. These insights are then compared with experimental conductance trends reported in ref. 44. After that, we evaluate thermoelectric properties through Seebeck coefficient calculations, highlighting how CQI or DQI impacts both conductance and thermoelectric performance.

3.1.1 Connectivity analysis. Before presenting the results of DFT calculations, we first discuss how the *meta* and *para* connectivities within the upper and lower branches of the macrocycles could be expected to influence their electrical conductance. For example, in Fig. 2a, starting from the left-most phenyl ring of **BMC1**, and traversing the upper branch from left to right, an electron would encounter a *para–meta–meta* series of connectivities, whereas an electron traversing the lower branch would encounter a *meta–meta–para* sequence. Since both branches contain two low-conductance *meta*-connected rings, we expect this macrocycle to have a low conductance. In contrast, the upper branch of **BMC2** possesses a *meta–meta–meta* series of connectivities, which should effectively block electron transport. On the other hand, the lower branch has a *para–meta–para* sequence. Since this contains only a single *meta* connectivity, we expect it to be more conductive than either of the branches of **BMC1**. Therefore, we expect **BMC2** to have a higher conductance than **BMC1**. The third macrocycle, **TMC3**, incorporates *para–para–meta* and *meta–para–para* connectivities in the upper and lower branches respectively. In common with the lower branch of **BMC2**, these have only a single *meta* connection and since there are two such branches, we expect **TMC3** to have a higher conductance than **BMC1** and **BMC2**. Finally, since **TMC4** has a high-conductance *para–para–para* lower branch, we expect this to have the highest conductance of all. To check these qualitative predictions, we now proceed to analyse the DFT-calculated transmission functions of each macrocycle. As an initial step, we conducted binding energy analyses of the sulfur–gold contacts.[51–53] These calculations verified that the anchoring geometries are consistent across all studied systems. The optimised Au–S bond lengths and binding energies, provided in the SI, Fig. S7, S8 and Table S3, support the formation of stable and reproducible sulfur–gold contacts. Fig. 3(a–d) show the electrode–molecule junction geometries for each system, illustrating the anchoring configurations employed in the transport simulations. The resulting transmission functions $T(E)$ for the four macrocycles are presented in Fig. 3e, where they are plotted against electron energy E, relative to the DFT-predicted Fermi energy E_F^{DFT}. In the case of **BMC1**, which features two *meta* connectivities in each branch, the DFT transmission function (blue curve) shows a clear sign of DQI, indicated by the presence of a dip in the transmission spectrum $T(E)$, within the HOMO–LUMO gap at an energy $E - E_F^{DFT} \approx 0.45$ eV. Likewise, **BMC2**, which has *meta–meta–meta* and *para–meta–para* branches, shows a similarly low transmission profile (red curve), with a DQI dip near $E - E_F^{DFT} \approx 0.3$ eV. In contrast, the thiophene-based macrocycle **TMC3**, with only a single *meta* connectivity in both branches respectively, has a higher transmission function within the gap than both **BMC1** and **BMC2**. Finally, **TMC4**, which possesses a branch with no *meta* connectivity, has the highest transmission function. These results agree with the above qualitative expectations, based on the number of *meta* connectivities within each macrocycle. To elucidate the physical mechanism governing the suppressed conductance in the 2,4-substituted isomers, we look beyond the energy levels of the frontier molecular orbitals (HOMO/LUMO) and examine the spatial distribution and phase relationship of the electronic pathways. The repositioning of the sulfur atom from the 2,5-position (CQI) to the 2,4-position (DQI) induces a change in the quantum interference (QI) pattern across the thiophene rings. While the

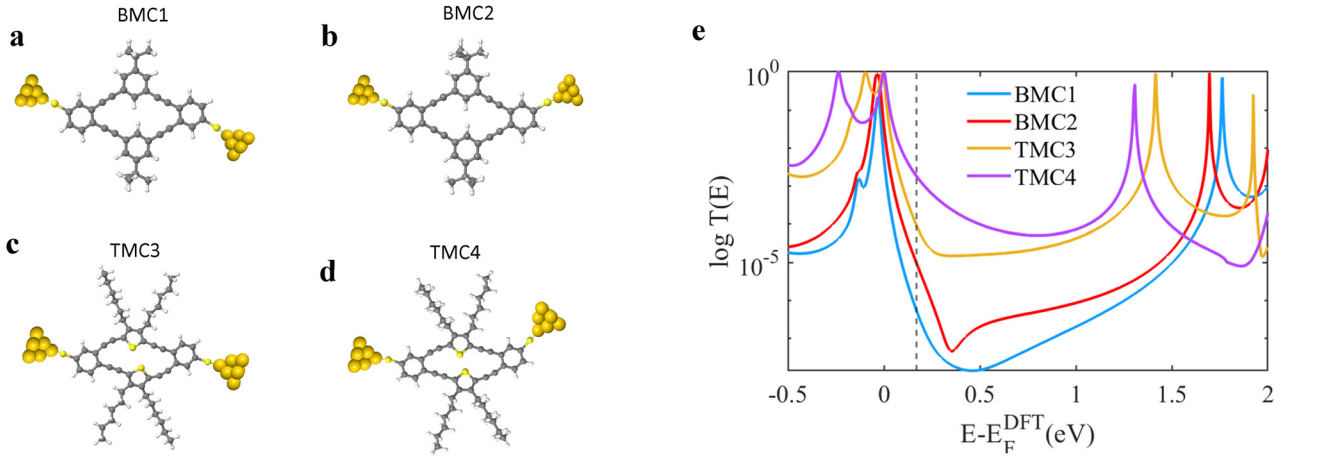

Fig. 3 (a)–(d) Optimized junction geometries of **BMC1**, **BMC2**, **TMC3**, and **TMC4** with gold electrodes attached at terminal sulfur atoms. (e) Transmission coefficients, $T(E)$, plotted as a function of energy in electron volts (eV) for the four macrocyclic molecules.

2,5-connectivity allows for a continuous electronic coupling through the pi-conjugated backbone, the 2,4-connectivity introduces a phase-reversal node within the HOMO–LUMO gap. Analysis of the electron/hole distribution reveals that in the DQI (2,4) configurations, the transmission amplitude is the result of a superposition of multiple pathways that interfere destructively at the exit anchor point. Specifically, the transmission function in DQI-modified **TMC3** and **TMC4** shows a marked suppression at the carbon–sulfur nodes, confirming that the reduction in transmission is a consequence of wavefunction cancellation rather than a simple increase in the tunneling barrier. This phase-driven suppression creates a sharp antiresonance in the transmission function $T(E)$. According to the Mott formula, the Seebeck coefficient is directly proportional to the energy derivative of the logarithm of $T(E)$. The dramatic enhancement of the Seebeck coefficient in DQI.4 (reaching 522.4 μV K^{-1} in **TMC4**) is thus mechanically explained by the extreme slope of the transmission curve near the Fermi level (E_F), where the proximity to the DQI dip maximizes the asymmetry of the electron–hole transport channels. This confirms that sulfur repositioning acts as a "phase-switch," enabling precise control over the interference-driven thermoelectric response.

3.1.2 Comparison with experimental data. We now compare these theoretical results with experimental measurements.[44] The theoretical conductance values were obtained using the Landauer formula, as described earlier in the Computational methods section, by evaluating the transmission coefficient at the Fermi energy. A summary of the experimental and theoretical conductance data is provided in Table S5 in the SI. Comparisons between theory and experiment in past studies have shown that the DFT-predicted Fermi energy E_F^{DFT} may not coincide with the Fermi energy E_F in the actual experiment. Therefore, we determine E_F by choosing a single value which gives the closest agreement between theory and experiment for all four molecules. The resulting E_F is shown as the dashed vertical line in Fig. 3e and differs slightly (by 0.2 eV) from the DFT-predicted value. Using this value for E_F, a comparison between the predicted conductances $G = G_0T(E_F)$ and the experimental values is shown in Fig. 4. In agreement with experiment, we find that the thiophene-based macrocycles (**TMC3** and **TMC4**) exhibit higher conductance than the benzene-based macrocycles (**BMC1** and **BMC2**), with conductances following the order **TMC4** ≈ **TMC3** > **BMC2** > **BMC1**.

3.1.3 Seebeck coefficient. Since experimental studies[44] did not assess the thermoelectric properties of these macrocycles, we now turn to an analysis of their Seebeck coefficients S.[54] The latter are of interest, because when a temperature difference ΔT is applied across a junction, it can generate a voltage difference ΔV given by $\Delta V = -S\Delta T$. Therefore a large value of S means that such molecules have an ability to convert heat directly into electricity, with no moving parts. If the slope of the transmission function is approximately constant within an energy range of order k_BT, centred on E_F, then the Seebeck coefficient is given by the Mott formula:

$$S = -\frac{\pi^2 k_B^2 T}{3e}\frac{\partial \ln(T(E))}{\partial E}\bigg|_{E=E_F} \quad (1)$$

This shows that Seebeck coefficients are proportional to the negative slopes of $\ln(T(E))$, evaluated at the Fermi energy. From Fig. 3e, at the crossing points between the vertical dashed line and the transmission curves, all slopes are negative and therefore we predict that all Seebeck coefficients are positive, consistent with HOMO-dominated transport. Combining these slopes with the Mott formula yields the following predictions

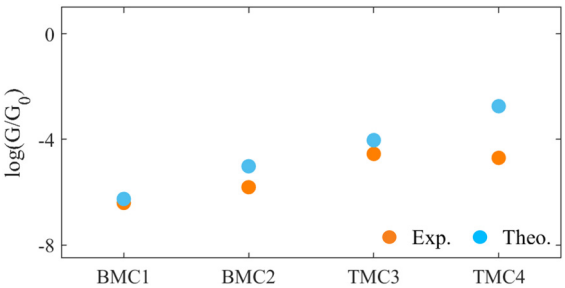

Fig. 4 Log-scale plot comparing experimental and theoretical conductances for the four macrocycles **BMC1**–**TMC4**.

for the Seebeck coefficients of **TMC4**, **TMC3**, **BMC2** and **BMC1** respectively: 300 μV K^{-1}, 527 μV K^{-1}, 628 μV K^{-1}, and 643 μV K^{-1}. Interestingly, this is the opposite order to their electrical conductances, with the lowest conductance molecule having the highest Seebeck coefficient and the highest conductance molecule having the lowest Seebeck coefficient. Such a trend has been noted for other molecular junctions.[55,56] More details and Seebeck coefficient curves can be found in the SI, Fig. S10. The predicted values of S are remarkably high. For example, a related study conducted by Hong *et al.*[57] investigated linear molecules with single thiophene or benzene branches and thioacetate as an anchoring group, yielding a Seebeck coefficient of approximately +7.97 μV K^{-1} for the thiophene-based molecule (2,5-TP-SAc) and an even lower value for the benzene-based variant (*para*-OPE3). In contrast, our molecules have multiple branches, which suggests that molecules with multiple pathways can significantly enhance thermoelectric performance. For more details regarding the comparison data between both cyclic and single-branch molecules, see the SI, Table S6.

While the role of molecular connectivity in governing quantum interference (QI) is well-documented in molecular electronics, our findings demonstrate a conceptual shift when moving from charge conductance to thermoelectric optimization. In standard molecular junctions, the focus is typically on the magnitude of the transmission function $T(E)$ at the Fermi level

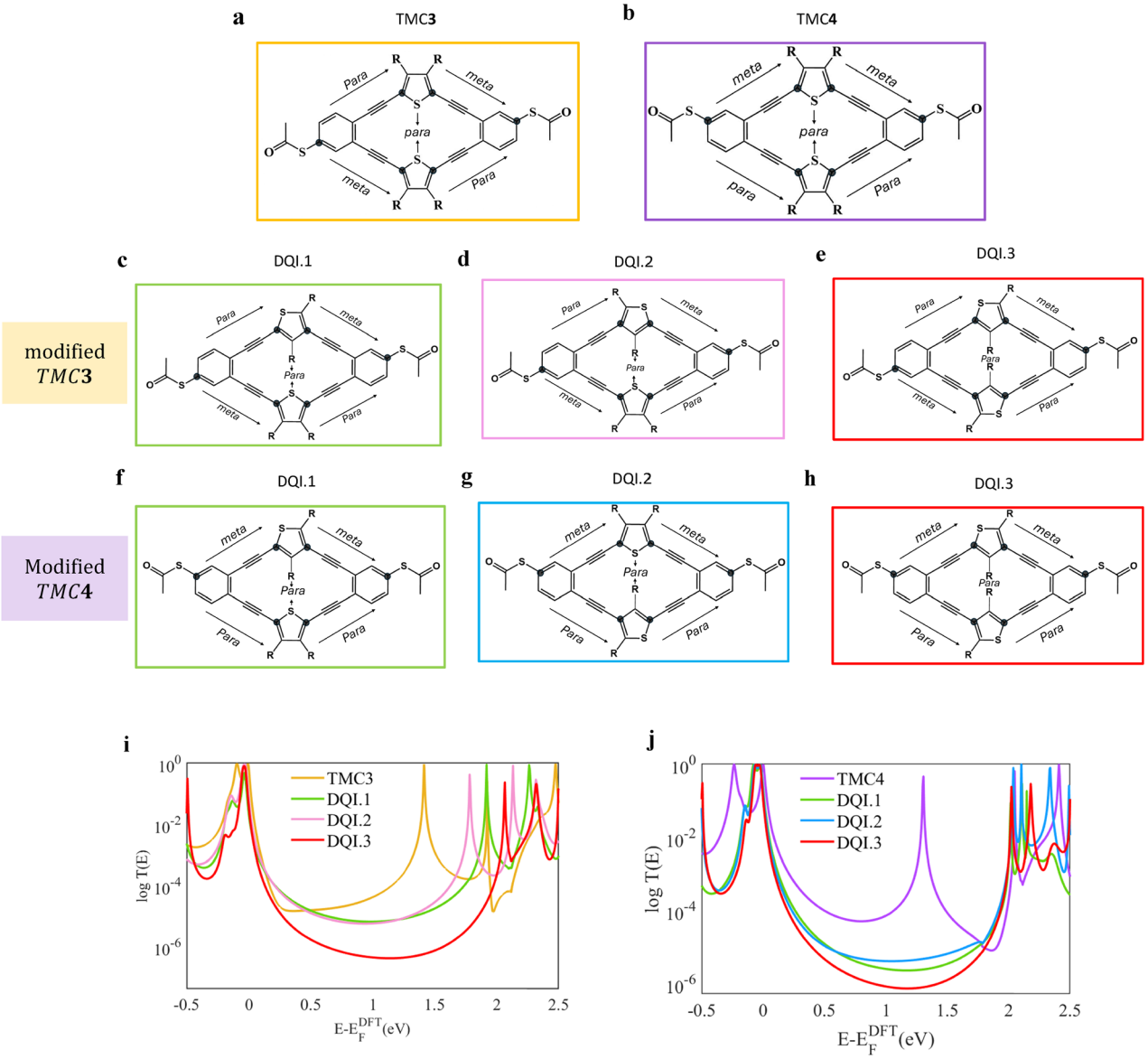

Fig. 5 Molecular structures and transmission results for **TMC3** and **TMC4** with different sulfur positions in the thiophene units. (a) Original structure of **TMC3**. (b) Original structure of **TMC4**. (c)–(e) Adjusted **TMC3** structures showing sulfur-position modifications in the thiophene units, labeled as **DQI.1**, **DQI.2**, and **DQI.3**, respectively. (f)–(h) Adjusted **TMC4** structures with corresponding sulfur-position modifications, labeled as **DQI.1**, **DQI.2**, and **DQI.3**, respectively. (i) and (j) Transmission coefficient curves for **TMC3** (panel i) and **TMC4** (panel j), comparing the original structures with the three sulfur-position modifications.

(E_F) to maximize conductance (G). However, the Seebeck coefficient (S) is governed by the energy derivative of the transmission, as described by the Mott formula (eqn (1)).

The ''design principle'' introduced here transcends simple ''on/off'' QI switching. We demonstrate that the specific positioning of heteroatoms in the DQI-1 to DQI-3 configurations does more than just permit transport; it induces a sharp antiresonance feature in close proximity to E_F. This proximity creates a significantly steeper transmission slope than those observed in single-branch analogues or previously studied thiophene derivatives.

Consequently, we achieve a Seebeck coefficient exceeding 500 μV K^{-1}, a result that would be inaccessible through standard constructive interference alone. This highlights a unique thermoelectric design rule: whereas electronic efficiency often seeks to maximize $T(E)$, thermoelectric efficiency in macrocycles relies on the strategic use of destructive interference to maximize the asymmetry of the transmission function. This distinction provides a new framework for utilizing multi-pathway molecules as high-performance thermoelectric materials rather than just molecular wires.

3.2 The effect of sulfur repositioning

The location of the 2–5 sulfur in the thiophene rings of **TMC3** and **TMC4** means that these rings exhibit CQI, whereas thiophene rings with 2–4 sulfurs exhibit DQI.[45] To explore the effect of repositioning the sulfur atoms within the thiophene rings of **TMC3** and **TMC4**, we start with molecule 3 (**TMC3**), which contains *meta–para–para* and *para–para–meta* branches. Fig. 5c–e show the three inequivalent molecular structures, obtained by repositioning the sulfurs to positions corresponding to DQI in the thiophene rings. Fig. 5i shows a comparison between their transmission functions and that of **TMC3**. In **DQI.1** and **DQI.2** (Fig. 5c and d), the shift in the sulfur atom of the upper branch creates DQI in the upper thiophene ring, leading to a reduction in transmission within the HOMO–LUMO gap compared with the original configuration. In **DQI.3** (Fig. 5e) the shift in the sulfur atom of the lower branch also creates DQI in the thiophene ring of the lower branch, which, as shown by the red curve in Fig. 5i, further decreases the transmission function within the gap. A similar *trans* is found in the corresponding modifications of **TMC4**, where (see Fig. 5j) introduction of a DQI thiophene in either the upper or lower branches lowers the transmission functions and the presence of DQI thiophenes in both branches lowers the transmission functions even further.

This approach offers a structurally minimal yet powerful method for tuning interference pathways, enabling precise control over electron transmission through single-molecule systems. Similar observations were reported experimentally by Chen *et al.*,[57] who compared two positional isomers of thiophene-based molecules—2,4-TP-SAc and 2,5-TP-SAc—and found that the conductance of the molecule with DQI (2,4-TP-SAc) was nearly two orders of magnitude lower than its CQI counterpart, despite having almost identical molecular lengths. These results confirm that positional changes in thiophene rings provide a robust strategy for switching between constructive and destructive QI, consistent with the behavior observed in our macrocyclic systems.

We also calculated the Seebeck coefficient for the modified sulfur positions. The results show relatively higher Seebeck values compared to the original structures. In **TMC3**, the DQI.4 configuration exhibits a Seebeck value of 583.6 μV K^{-1}, which is about 50 μV K^{-1} higher than that of the original sulfur position (527 μV K^{-1}). In **TMC4**, the DQI.4 structure shows a much larger increase, reaching 522.4 μV K^{-1} compared to 300 μV K^{-1} in the original molecule, more than 200 μV K^{-1} higher. Further Seebeck values for the other DQI configurations are summarized in Table S7, and the corresponding Seebeck curves are presented in Fig. S11. In conclusion, this work demonstrates that macrocyclic molecular junctions with engineered connectivities represent a highly versatile platform for controlling quantum interference and enhancing thermoelectric performance at the single-molecule level. By comparing experimental data with DFT calculations, we have shown that the distinct conductance states arising from mixed connectivities are governed by QI effects. Beyond explaining conductance trends, we have predicted a markedly superior thermopower in these multi-pathway macrocyclic systems compared to standard molecular wires. Most significantly, we identified the repositioning of sulfur atoms within the thiophene rings as a powerful and precise design strategy. Our findings, which bridge intuitive theoretical models with predictive device-level properties, provide a roadmap for the rational design of high-Seebeck-coefficient, QI-based molecular thermoelectrics.

Conflicts of interest

There are no conflicts to declare.

Data availability

In this work, we use the following codes. (1) Siesta code used to predict the Hamiltonian of each system used in this study, which is located in **https://gitlab.com/siesta-project/siesta/-/releases**. (2) GOLLUM software is used to find the transmission coefficient. **https://www.gollumcode.com/**. (3) Conductance, Seebeck coefficient, and other parameters are calculated using the own Fortran code available upon request.

Supplementary information (SI) is available. The SI provides details about optimised DFT structures of isolated molecules, binding energy, transmission coefficient and Seebeck coefficient. See DOI: **https://doi.org/10.1039/d5qm00845j**.

Acknowledgements

This work was supported by the UK EPSRC (grant QMol EP/X026876/1). A. K. I. acknowledges the Leverhulme Trust for the Early Career Fellowship ECF-2020-638 and financial support from the Tikrit University (Iraq) and the Iraqi Ministry of Higher Education (SL-20). M. A., A. A., and B. A., H. A., A. A.

are grateful for financial assistance from Hafr Al Batin University, Prince Sattam bin Abdulaziz University, Al-Kharj, and Northern Border University, Shaqra University, the Islamic University of Madinah and the Saudi Ministry of Education.

References

1 B. Huang, X. Liu, Y. Yuan, Z.-W. Hong, J.-F. Zheng, L.-Q. Pei, Y. Shao, J.-F. Li, X.-S. Zhou, J.-Z. Chen, S. Jin and B.-W. Mao, Controlling and Observing Sharp-Valleyed Quantum Interference Effect in Single Molecular Junctions, *J. Am. Chem. Soc.*, 2018, **140**(50), 17685–17690, DOI: **10.1021/jacs.8b10450**.

2 J. M. Hamill, A. Ismael, A. Al-Jobory, T. L. R. Bennett, M. Alshahrani, X. Wang, M. Akers-Douglas, L. A. Wilkinson, B. J. Robinson, N. J. Long, C. Lambert and T. Albrecht, Quantum Interference and Contact Effects in the Thermoelectric Performance of Anthracene-Based Molecules, *J. Phys. Chem. C*, 2023, **127**(15), 7484–7491, DOI: **10.1021/acs.jpcc.3c00069**.

3 K. Reznikova, C. Hsu, W. M. Schosser, A. Gallego, K. Beltako, F. Pauly, H. S. J. van der Zant and M. Mayor, Substitution Pattern Controlled Quantum Interference in [2.2]Paracyclophane-Based Single-Molecule Junctions, *J. Am. Chem. Soc.*, 2021, **143**(34), 13944–13951, DOI: **10.1021/jacs.1c06966**.

4 X. Li, Y. Zheng, Y. Zhou, Z. Zhu, J. Wu, W. Ge, Y. Zhang, Y. Ye, L. Chen, J. Shi, J. Liu, J. Bai, Z. Liu and W. Hong, Supramolecular Transistors with Quantum Interference Effect, *J. Am. Chem. Soc.*, 2023, **145**(39), 21679–21686, DOI: **10.1021/jacs.3c08615**.

5 A. K. Ismael, A. Al-Jobory, I. Grace and C. J. Lambert, Discriminating Single-Molecule Sensing by Crown-Ether-Based Molecular Junctions, *J. Chem. Phys.*, 2017, **146**(6), 064704, DOI: **10.1063/1.4975771**.

6 G. C. Solomon, D. Q. Andrews, R. H. Goldsmith, T. Hansen, M. R. Wasielewski, R. P. Van Duyne and M. A. Ratner, Quantum Interference in Acyclic Systems: Conductance of Cross-Conjugated Molecules, *J. Am. Chem. Soc.*, 2008, **130**(51), 17301–17308, DOI: **10.1021/ja8044053**.

7 M. Thoss and F. Evers, Perspective: Theory of Quantum Transport in Molecular Junctions, *J. Chem. Phys.*, 2018, **148**(3), 030901, DOI: **10.1063/1.5003306**.

8 C. Tang, L. Huang, S. Sangtarash, M. Noori, H. Sadeghi, H. Xia and W. Hong, Reversible Switching between Destructive and Constructive Quantum Interference Using Atomically Precise Chemical Gating of Single-Molecule Junctions, *J. Am. Chem. Soc.*, 2021, **143**(25), 9385–9392, DOI: **10.1021/jacs.1c00928**.

9 L. A. Wilkinson, T. L. R. Bennett, I. M. Grace, J. Hamill, X. Wang, S. Au-Yong, A. Ismael, S. P. Jarvis, S. Hou, T. Albrecht, L. F. Cohen, C. Lambert, B. J. Robinson and N. J. Long, Assembly, Structure and Thermoelectric Properties of 1,1′-Dialkynylferrocene 'Hinges', *Chem. Sci.*, 2022, **13**(28), 8380–8387, DOI: **10.1039/D2SC00861K**.

10 X. Li, Z. Tan, X. Huang, J. Bai, J. Liu and W. Hong, Experimental Investigation of Quantum Interference in Charge Transport through Molecular Architectures, *J. Mater. Chem. C*, 2019, **7**(41), 12790–12808, DOI: **10.1039/C9TC02626F**.

11 A. Ismael, A. Al-Jobory, X. Wang, A. Alshehab, A. Almutlg, M. Alshammari, I. Grace, T. L. R. Benett, L. A. Wilkinson, B. J. Robinson, N. J. Long and C. Lambert, Molecular-Scale Thermoelectricity: As Simple as 'ABC', *Nanoscale Adv.*, 2020, **2**(11), 5329–5334, DOI: **10.1039/D0NA00772B**.

12 M. Taniguchi, M. Tsutsui, R. Mogi, T. Sugawara, Y. Tsuji, K. Yoshizawa and T. Kawai, Dependence of Single-Molecule Conductance on Molecule Junction Symmetry, *J. Am. Chem. Soc.*, 2011, **133**(30), 11426–11429, DOI: **10.1021/ja2033926**.

13 S. V. Aradhya and L. Venkataraman, Single-Molecule Junctions beyond Electronic Transport, *Nat. Nanotechnol.*, 2013, **8**(6), 399–410, DOI: **10.1038/nnano.2013.91**.

14 T. Markussen, R. Stadler and K. S. Thygesen, The Relation between Structure and Quantum Interference in Single Molecule Junctions, *Nano Lett.*, 2010, **10**(10), 4260–4265, DOI: **10.1021/nl101688a**.

15 P. Sautet and C. Joachim, Electronic Interference Produced by a Benzene Embedded in a Polyacetylene Chain, *Chem. Phys. Lett.*, 1988, **153**(6), 511–516, DOI: **10.1016/0009-2614(88)85252-7**.

16 K. Yoshizawa, T. Tada and A. Staykov, Orbital Views of the Electron Transport in Molecular Devices, *J. Am. Chem. Soc.*, 2008, **130**(29), 9406–9413, DOI: **10.1021/ja800638t**.

17 R. Baer and D. Neuhauser, Phase Coherent Electronics: A Molecular Switch Based on Quantum Interference, *J. Am. Chem. Soc.*, 2002, **124**(16), 4200–4201, DOI: **10.1021/ja016605s**.

18 Y. Fan, S. Tao, S. Pitié, C. Liu, C. Zhao, M. Seydou, Y. J. Dappe, P. J. Low, R. J. Nichols and L. Yang, Destructive Quantum Interference in Meta -Oligo(Phenyleneethynylene) Molecular Wires with Gold–Graphene Heterojunctions, *Nanoscale*, 2024, **16**(1), 195–204, DOI: **10.1039/D3NR04012G**.

19 R. Almughathawi, S. Hou, Q. Wu and C. J. Lambert, Signatures of Topological States in Conjugated Macrocycles, *Nano Lett.*, 2024, **24**(16), 4972–4978, DOI: **10.1021/acs.nanolett.3c04796**.

20 T. L. R. Bennett, M. Alshammari, S. Au-Yong, A. Almutlg, X. Wang, L. A. Wilkinson, T. Albrecht, S. P. Jarvis, L. F. Cohen, A. Ismael, C. J. Lambert, B. J. Robinson and N. J. Long, Multi-Component Self-Assembled Molecular-Electronic Films: Towards New High-Performance Thermoelectric Systems, *Chem. Sci.*, 2022, **13**(18), 5176–5185, DOI: **10.1039/D2SC00078D**.

21 G. Yang, S. Sangtarash, Z. Liu, X. Li, H. Sadeghi, Z. Tan, R. Li, J. Zheng, X. Dong, J. Liu, Y. Yang, J. Shi, Z. Xiao, G. Zhang, C. Lambert, W. Hong and D. Zhang, Protonation Tuning of Quantum Interference in Azulene-Type Single-Molecule Junctions, *Chem. Sci.*, 2017, **8**(11), 7505–7509, DOI: **10.1039/C7SC01014A**.

22 A. K. Ismael, I. Grace and C. J. Lambert, Increasing the Thermopower of Crown-Ether-Bridged Anthraquinones,

Nanoscale, 2015, **7**(41), 17338–17342, DOI: **10.1039/C5NR04907E**.

23 A. A. Kocherzhenko, F. C. Grozema and L. D. A. Siebbeles, Charge Transfer Through Molecules with Multiple Pathways: Quantum Interference and Dephasing, *J. Phys. Chem. C*, 2010, **114**(17), 7973–7979, DOI: **10.1021/jp9117216**.

24 A. A. Kocherzhenko, L. D. A. Siebbeles and F. C. Grozema, Chemically Gated Quantum-Interference-Based Molecular Transistor, *J. Phys. Chem. Lett.*, 2011, **2**(14), 1753–1756, DOI: **10.1021/jz200535j**.

25 G. C. Solomon, D. Q. Andrews, T. Hansen, R. H. Goldsmith, M. R. Wasielewski, R. P. Van Duyne and M. A. Ratner, Understanding Quantum Interference in Coherent Molecular Conduction, *J. Chem. Phys.*, 2008, **129**(5), 054701, DOI: **10.1063/1.2958275**.

26 D. M. Cardamone, C. A. Stafford and S. Mazumdar, Controlling Quantum Transport through a Single Molecule, *Nano Lett.*, 2006, **6**(11), 2422–2426, DOI: **10.1021/nl0608442**.

27 C. J. Lambert, Basic Concepts of Quantum Interference and Electron Transport in Single-Molecule Electronics, *Chem. Soc. Rev.*, 2015, **44**(4), 875–888, DOI: **10.1039/C4CS00203B**.

28 C. J. Lambert and S.-X. Liu, A Magic Ratio Rule for Beginners: A Chemist's Guide to Quantum Interference in Molecules, *Chem. – Eur. J.*, 2018, **24**(17), 4193–4201, DOI: **10.1002/chem.201704488**.

29 W.-Y. Lo, N. Zhang, Z. Cai, L. Li and L. Yu, Beyond Molecular Wires: Design Molecular Electronic Functions Based on Dipolar Effect, *Acc. Chem. Res.*, 2016, **49**(9), 1852–1863, DOI: **10.1021/acs.accounts.6b00305**.

30 A. Troisi and M. A. Ratner, Molecular Signatures in the Transport Properties of Molecular Wire Junctions: What Makes a Junction ''Molecular''?, *Small*, 2006, **2**(2), 172–181, DOI: **10.1002/smll.200500201**.

31 A. S. Blum, J. G. Kushmerick, D. P. Long, C. H. Patterson, J. C. Yang, J. C. Henderson, Y. Yao, J. M. Tour, R. Shashidhar and B. R. Ratna, Molecularly Inherent Voltage-Controlled Conductance Switching, *Nat. Mater.*, 2005, **4**(2), 167–172, DOI: **10.1038/nmat1309**.

32 S. J. van der Molen, J. Liao, T. Kudernac, J. S. Agustsson, L. Bernard, M. Calame, B. J. van Wees, B. L. Feringa and C. Schönenberger, Light-Controlled Conductance Switching of Ordered Metal−Molecule−Metal Devices, *Nano Lett.*, 2009, **9**(1), 76–80, DOI: **10.1021/nl802487j**.

33 C. Jia, A. Migliore, N. Xin, S. Huang, J. Wang, Q. Yang, S. Wang, H. Chen, D. Wang, B. Feng, Z. Liu, G. Zhang, D.-H. Qu, H. Tian, M. A. Ratner, H. Q. Xu, A. Nitzan and X. Guo, Covalently Bonded Single-Molecule Junctions with Stable and Reversible Photoswitched Conductivity, *Science*, 2016, **352**(6292), 1443–1445, DOI: **10.1126/science.aaf6298**.

34 A. K. Ismael, L. Rincón-García, C. Evangeli, P. Dallas, T. Alotaibi, A. A. Al-Jobory, G. Rubio-Bollinger, K. Porfyrakis, N. Agraït and C. J. Lambert, Exploring Seebeck-Coefficient Fluctuations in Endohedral-Fullerene, Single-Molecule Junctions, *Nanoscale Horiz.*, 2022, **7**(6), 616–625, DOI: **10.1039/D1NH00527H**.

35 T. Alotaibi, M. Alshahrani, M. Alshammari, M. Alotaibi, T. A. M. Taha, A. A. Al-Jobory and A. Ismael, Orientational Effects and Molecular-Scale Thermoelectricity Control, *ACS Omega*, 2024, **9**(27), 29537–29543, DOI: **10.1021/acsomega.4c02141**.

36 H. Sadeghi, S. Sangtarash and C. J. Lambert, Oligoyne Molecular Junctions for Efficient Room Temperature Thermoelectric Power Generation, *Nano Lett.*, 2015, **15**(11), 7467–7472, DOI: **10.1021/acs.nanolett.5b03033**.

37 Y. Kim, W. Jeong, K. Kim, W. Lee and P. Reddy, Electrostatic Control of Thermoelectricity in Molecular Junctions, *Nat. Nanotechnol.*, 2014, **9**(11), 881–885, DOI: **10.1038/nnano.2014.209**.

38 J. Koga, Y. Tsuji and K. Yoshizawa, Orbital Control of Single-Molecule Conductance Perturbed by π-Accepting Anchor Groups: Cyanide and Isocyanide, *J. Phys. Chem. C*, 2012, **116**(38), 20607–20616, DOI: **10.1021/jp3068156**.

39 M. Kiguchi and S. Kaneko, Single Molecule Bridging between Metal Electrodes, *Phys. Chem. Chem. Phys.*, 2013, **15**(7), 2253–2267, DOI: **10.1039/C2CP43960C**.

40 D. Sánchez-Portal, P. Ordejón, E. Artacho and J. M. Soler, Density-Functional Method for Very Large Systems with LCAO Basis Sets, *Int. J. Quantum Chem.*, 1997, **65**(5), 453–461, DOI: **10.1002/(SICI)1097-461X(1997)65:5%253C453::AID-QUA9%253E3.0.CO;2-V**.

41 B. T. Pickup and P. W. Fowler, An Analytical Model for Steady-State Currents in Conjugated Systems, *Chem. Phys. Lett.*, 2008, **459**(1), 198–202, DOI: **10.1016/j.cplett.2008.05.062**.

42 M. Noori, A. C. Aragonès, G. Di Palma, N. Darwish, S. W. D. Bailey, Q. Al-Galiby, I. Grace, D. B. Amabilino, A. González-Campo, I. Díez-Pérez and C. J. Lambert, Tuning the Electrical Conductance of Metalloporphyrin Supramolecular Wires, *Sci. Rep.*, 2016, **6**, 37352, DOI: **10.1038/srep37352**.

43 Y. Yang, M. Gantenbein, A. Alqorashi, J. Wei, S. Sangtarash, D. Hu, H. Sadeghi, R. Zhang, J. Pi, L. Chen, X. Huang, R. Li, J. Liu, J. Shi, W. Hong, C. J. Lambert and M. R. Bryce, Heteroatom-Induced Molecular Asymmetry Tunes Quantum Interference in Charge Transport through Single-Molecule Junctions, *J. Phys. Chem. C*, 2018, **122**(26), 14965–14970, DOI: **10.1021/acs.jpcc.8b03023**.

44 S. L. Heim, A. Gallego, V. Bertozzi, S. van der Poel, L. Ornago, A. Prescimone, H. S. J. van der Zant and M. Mayor, Design and Synthesis of Multipath Compact Cyclophanes for Quantum Interference Studies, *Eur. J. Org. Chem.*, 2024, (48), e202400914, DOI: **10.1002/ejoc.202400914**.

45 J. Bai, A. Daaoub, S. Sangtarash, X. Li, Y. Tang, Q. Zou, H. Sadeghi, S. Liu, X. Huang, Z. Tan, J. Liu, Y. Yang, J. Shi, G. Mészáros, W. Chen, C. Lambert and W. Hong, Anti-Resonance Features of Destructive Quantum Interference in Single-Molecule Thiophene Junctions Achieved by Electrochemical Gating, *Nat. Mater.*, 2019, **18**(4), 364–369, DOI: **10.1038/s41563-018-0265-4**.

46 J. M. Soler, E. Artacho, J. D. Gale, A. Garcia, J. Junquera, P. Ordejon and D. Sanchez-Portal, The SIESTA Method for

Ab Initio Order-N Materials Simulation, *J. Phys.: Condens. Matter*, 2002, **14**(11), 2745–2779, DOI: **10.1088/0953-8984/14/11/302**.

47 E. Artacho, E. Anglada, O. Diéguez, J. D. Gale, A. García, J. Junquera, R. M. Martin, P. Ordejón, J. M. Pruneda, D. Sánchez-Portal and J. M. Soler, The SIESTA Method; Developments and Applicability, *J. Phys.: Condens. Matter*, 2008, **20**(6), 064208, DOI: **10.1088/0953-8984/20/6/064208**.

48 R. J. Davidson, D. C. Milan, O. A. Al-Owaedi, A. K. Ismael, R. J. Nichols, S. J. Higgins, C. J. Lambert, D. S. Yufit and A. Beeby, Conductance of 'Bare-Bones' Tripodal Molecular Wires, *RSC Adv.*, 2018, **8**(42), 23585–23590, DOI: **10.1039/C8RA01257A**.

49 A. Markin, A. K. Ismael, R. J. Davidson, D. C. Milan, R. J. Nichols, S. J. Higgins, C. J. Lambert, Y.-T. Hsu, D. S. Yufit and A. Beeby, Conductance Behavior of Tetraphenyl-Aza-BODIPYs, *J. Phys. Chem. C*, 2020, **124**(12), 6479–6485, DOI: **10.1021/acs.jpcc.9b10232**.

50 A. Alshehab and A. K. Ismael, Impact of the Terminal End-Group on the Electrical Conductance in Alkane Linear Chains, *RSC Adv.*, 2023, **13**(9), 5869–5873, DOI: **10.1039/D3RA00019B**.

51 N. Kobko and J. J. Dannenberg, Effect of Basis Set Superposition Error (BSSE) upon Ab Initio Calculations of Organic Transition States, *J. Phys. Chem. A*, 2001, **105**(10), 1944–1950, DOI: **10.1021/jp001970b**.

52 C. D. Sherrill, Counterpoise Correction and Basis Set Superposition Error.

53 S. F. Boys and F. Bernardi, The Calculation of Small Molecular Interactions by the Differences of Separate Total Energies. Some Procedures with Reduced Errors, *Mol. Phys.*, 1970, **19**(4), 553–566, DOI: **10.1080/00268977000101561**.

54 Q. H. Al-Galiby, H. Sadeghi, D. Zsolt Manrique and C. J. Lambert, Tuning the Seebeck Coefficient of Naphthalenediimide by Electrochemical Gating and Doping, *Nanoscale*, 2017, **9**(14), 4819–4825, DOI: **10.1039/C7NR00571G**.

55 A. K. Ismael and C. J. Lambert, Molecular-Scale Thermoelectricity: A Worst-Case Scenario, *Nanoscale Horiz.*, 2020, **5**(7), 1073–1080, DOI: **10.1039/D0NH00164C**.

56 X. Wang, A. Ismael, B. Alanazi, A. Al-Jobory, J. Wang and C. J. Lambert, High Seebeck Coefficient from Isolated Oligo-Phenyl Arrays on Single Layered Graphene *via* Stepwise Assembly, *J. Mater. Chem. C*, 2023, **11**(42), 14652–14660, DOI: **10.1039/D3TC02842A**.

57 H. Chen, Y. Chen, H. Zhang, W. Cao, C. Fang, Y. Zhou, Z. Xiao, J. Shi, W. Chen, J. Liu and W. Hong, Quantum Interference Enhanced Thermopower in Single-Molecule Thiophene Junctions, *Chin. Chem. Lett.*, 2022, **33**(1), 523–526, DOI: **10.1016/j.cclet.2021.06.052**.